Accepted Manuscript

Impedance measurements on an Engineered Cementitious Composite: A critical evaluation of testing protocols

Benny Suryanto, Hideaki Takaoka, W. John McCater, Danah Saraireh, Hussameldin Taha

PII: S0263-2241(18)30692-4
DOI: https://doi.org/10.1016/j.measurement.2018.07.066
Reference: MEASUR 5750

To appear in: *Measurement*

Received Date: 14 September 2017
Revised Date: 5 April 2018
Accepted Date: 21 July 2018

Please cite this article as: B. Suryanto, H. Takaoka, W.J. McCater, D. Saraireh, H. Taha, Impedance measurements on an Engineered Cementitious Composite: A critical evaluation of testing protocols, *Measurement* (2018), doi: https://doi.org/10.1016/j.measurement.2018.07.066

Impedance measurements on an Engineered Cementitious Composite: A critical evaluation of testing protocols

Benny Suryanto[1]*, Hideaki Takaoka[1,2], W. John McCater[1], Danah Saraireh[1], Hussameldin Taha[1]

[1]School of Energy, Geoscience, Infrastructure and Society,

Heriot-Watt University,

Edinburgh, EH14 4AS,

United Kingdom,

[2] Civil Engineering Technology Department,

International Division, Shimizu Corporation,

Chuo-ku, Tokyo 104-8370,

Japan,

* Corresponding Author

E-mail: b.suryanto@hw.ac.uk

Tel: +44 (0)131 451 3817

Fax: +44 (0)131 451 4617

Abstract

An end-to-end (two-point) electrical measurement technique is traditionally employed in evaluating the bulk resistivity of hardened cementitious materials. This testing methodology is critically evaluated by studying the electrical impedance of an engineered cementitious composite (ECC), using cuboidal specimens with four different dimensions viz. 50mm, 70mm, 100mm and 150mm. In the present work, the impedance response (in the form of Nyquist plots) of the ECC specimens was measured over the frequency range 1Hz–10MHz via two external plate-electrodes placed at opposite faces of each specimen. A conductive gel, or saturated, synthetic sponges inserted between the plate/specimen interface were used as the electrode-specimen contacting medium. It is shown that the sponge contacting medium introduced a spurious response which was detectable across the entire frequency range and was particularly evident in specimens with smaller electrode contact area and in specimens with air-voids present on the contact surface. This effect was considerably reduced when either the conductive gel or sponges saturated with highly-conductive liquid was used. It is also shown that the true bulk resistivity of the material, identified from the Nyquist plot, can be *evaluated* by subtracting the resistivity of the sponge itself from the bulk resistivity of the ECC with the sponges present. Benchmarking studies were also undertaken on specimens with an embedded electrode arrangement.

Keywords: Engineered cementitious composite; electrical impedance; bulk resistivity; two-point measurements; electrodes; surface quality.

1. Introduction

Over the last two decades, a considerable amount of research has been directed towards the development of the next generation of cementitious materials. One such development is the engineered cementitious composite (ECC), which is known for its distinctive, high tensile strain capacity and its inherent ability to maintain crack widths below 0.1 mm [1]. The high tensile ductility is as a direct result of the formation of multiple micro-cracks instead of macro-cracks, as generally exhibited by reinforced concrete when subjected to tensile stresses beyond its elastic limit. It has been shown that the restricted crack opening of ECC ensures that the resistance of the material to moisture and ionic ingress (e.g. chlorides from de-icing salts) remains within an acceptable range [2, 3]. The controllable crack width characteristic has also been shown to promote autogenous crack healing [4, 5] thereby enhancing durability by protection of the reinforcing steel against corrosion [6].

To gain better insights into the durability of this novel composite, studies have been undertaken to assess its intrinsic permeation properties, including permeability [7], sorptivity [8] and diffusion [3, 9]. However, with an increased emphasis on performance-based design for durability, there is an inevitable need and, indeed, a growing interest to relate the desired, in-service performance of cementitious materials to an easily measurable parameter through an appropriate performance-based test [10]. Given that the underlying mechanism associated with permeability and diffusion is analogous to the flow of current under a potential gradient (hence, electrical conductivity, or its reciprocal, resistivity), increasing attention is now focussing on the electrical properties of cementitious systems (i.e. concrete) and utilisation of these properties as a *durability indicator* (see, for example, [11-13]).

To measure the electrical properties of cementitious systems, two- or four- electrode configurations are generally employed. In a two-electrode (or two-point) arrangement, the electrodes are either embedded within a test specimen at the time of casting [14-18] or placed externally against two opposite faces of a hardened sample [19-24], although the combination of the two has also been used to form a four-electrode arrangement [25, 26]. Other two-point electrode arrangements which have been used include the multi-electrode array which is positioned within the cover-zone of reinforced concrete at the time of casting [27, 28], and a multi-electrode system in which the electrodes are arranged externally along the perimeter of an object [29, 30]. The main advantage of using embedded electrodes arises primarily from the intimate contact of the electrodes with the surrounding material, allowing measurements to be taken virtually continuously over an extended period of time under a simulated or real-life environment [12, 27, 28]. Measurements are also technically simple and straightforward to undertake, and yield results which are easy to interpret. Despite these advantages, additional sample preparation is required prior to casting such as fabrication and positioning of electrodes within individual test specimen.

In a situation where the measurement of a large number of test specimens is required, such as during regular and frequent quality control or performance/durability testing, it may be desirable to use the external electrode configuration. In general, this involves the use of two metallic electrodes, typically stainless steel, placed at opposite faces of a prismatic test specimen with saturated sponges used to provide an intimate contact [19-24]. In this arrangement, no additional sample preparation is required and the same electrodes can be used for repeated measurements. Also, with this arrangement, it would be advantageous to use standard cubes or cylinders for electrical measurements which are currently used for compressive strength testing [31-35]. It has been recently shown that the electrode-specimen

contact region can, however, have a dominant influence on the measured response at low-frequencies and mask the actual bulk response [25, 26]. Failing to consider this spurious effect could, potentially, move the performance of concrete from one durability classification into another (see, for example the classification presented in Table 1). This is particularly relevant as low test-frequencies have been routinely used for bulk resistivity measurements; for example, 13 Hz [20, 24], 108 Hz [11], 128 Hz [19], 107 Hz and 120 Hz [38] and 1 kHz [21].

In the present paper, the two-electrode arrangement employing external plate-electrodes is applied to ECC, with the intention of developing a simple measurement technique which could be further exploited to assess the durability performance of this newly developed cementitious system. In developing this technique, it is necessary to firstly study factors influencing the bulk electrical properties; some of the factors investigated in the present work include specimen size, contacting medium, quality of the contacting surface and test frequency. The extent to which these factors impact the bulk electrical properties are evaluated by obtaining the electrical response (Nyquist plot) of the complete system (test specimen and contacting medium) over a wide frequency range (viz, 1Hz–10MHz). Whilst the *end-to-end* test arrangement has been extensively employed for ordinary concrete [19-26], it is expected that due to the high binder content used in ECC, the composite would exhibit lower impedance values which would increase the contribution of the electrode-specimen contacting medium to the bulk response. The multi-frequency measurements are, therefore, undertaken to clarify this aspect and allow optimization of the frequency in the development of single-frequency measurement protocols. Additional measurements on specimens with embedded electrodes are also undertaken to provide benchmark data.

2. Experimental Program

2.1 Materials

The mix proportion for the ECC used in this work is presented in Table 2. The water/binder (w/b) ratio was fixed at 0.28 by mass and the binder comprised Portland cement CEM I 52.5N to EN197-1 [39] and fine fly-ash (Superpozz SV80 from Scotash) which were mixed at a ratio of 1:1.8 by mass (i.e. a 64.3% replacement level). The aggregate used in the mix was fine silica sand (RH110 from Minerals Marketing Ltd.) with an average particle size of 120μm, which was added at a sand-to-cement ratio of 0.9 by mass. The oxide composition of these materials is provided in Table 3. Polyvinyl alcohol (PVA) fibers (RECS15 from Kuraray) were also added to the mix at a fixed dosage of 2% by total volume. The PVA fibers had an average diameter of 39μm, an average length of 12mm and an average tensile strength of 1.6GPa. To facilitate uniform fibre dispersion, a polycarboxylate high-range water-reducing admixture (MasterGlenium ACE499 from BASF) was added at a fixed dosage rate of 1% by mass of cement.

2.2. Sample Preparation

A Hobart planetary motion mixer, with a working capacity of 6 liters, was used to prepare the test specimens in three batches of 5 liters. As summarized in Table 4, a total of 18 specimens were cast in the first two batches: six 50mm cubes, six 70mm cubes and six 100mm cubes. The first batch specimens were used for compressive strength tests, whereas the second batch was used for electrical measurements. Six additional specimens were produced in the third batch: three 50mm cubes for compressive strength tests, one 150mm cube and two 40×40×160mm prisms for electrical measurements. Each prism had a pair of 45×65×2mm (thick) perforated stainless steel electrodes embedded 140mm apart, to ensure intimate bonding between the specimen and electrodes. It noteworthy that whilst it was possible to

produce only one 150mm cube in the last batch to avoid overloading the mixer, it was possible to produce two additional prisms from the same batch for benchmarking electrical measurements. The density and mean 28-day compressive strengths determined from three representative specimen dimensions are presented in Table 5.

All cuboidal specimens were cast in steel molds whereas the prisms were cast in a three-gang polystyrene mold. Immediately after casting, the top surface of each mold was covered with polyethylene sheeting to minimize the evaporation of water. The specimens were demolded after 24h and then placed in a curing tank stored in a temperature controlled laboratory environment (22±1^{o}C) until required for testing. For illustrative purposes, results are presented after 28- and 35-days continuous curing.

2.3. Electrical property measurements and data processing

A Solartron 1260 frequency response analyzer was employed to obtain the impedance of the cement composite over the frequency range 1Hz-10MHz. The impedance was recorded at 20 frequency points per decade in voltage drive mode, with relatively low signal amplitude of 350 mV to reduce lead inductive effects at the higher frequencies. This particular amplitude was chosen to also match the value used in previous studies including the field tests [12, 13, 16, 25–28]. It took approximately 4 minutes to complete one measurement sweep. All measurements were undertaken in a temperature-controlled laboratory (22±1°C).

Prior to electrical measurement, each specimen was removed from the curing tank and the surface was surface-dried with a paper towel to negate any surface conduction effects. In the *end-to-end* measurements, two external stainless steel (s/s) plate-electrodes were placed at two opposite surfaces of the specimen (see Figures 1(a) and (b)). To ensure intimate contact

between the electrodes and the specimen, either a thin layer (~2mm thick) of conductive gel (Spectra 360) or a pair of saturated synthetic sponges (see Figure 1(b)) was used. Each sponge had a thickness of 4mm, which reduced to ~3mm after being squeezed, and planar dimensions similar to the test specimen; this sponge was inserted between the plate/specimen interface. In this work, the following liquids were used to saturate the sponges:

(i) mains tap-water, with resistivity of ~160 Ωm; and

(ii) a saturated calcium hydroxide solution, with resistivity of ~8 Ωm.

A mass was then placed on the center of the upper electrode to give, together with the mass of the specimen, a uniform pressure of ~3.7kPa to the lower electrode. The following masses were used when testing the four different specimen dimensions: 2.1kg (150mm), 1.9kg (100mm), 1.2kg (70mm) and 0.7kg (50mm) (see Figure 1(b)). As the mass was applied, excess liquid squeezed out from the sponges and was removed with a paper towel.

Electrical measurements were undertaken by connecting the upper and lower electrodes to the voltage high/low and current output/input terminals in the Solartron analyzer via individually screened BNC coaxial cables, with connection at the electrodes by means of alligator clips (see Figures 1(b) and 2(b)). Two commercially available software packages (Schriber Associates: ZPlot and ZView) were used for experimental control and data acquisition. Lead inductive effects were nulled from the measured impedance data using an *open*- and *closed*-circuit calibration procedure implemented in an Excel spreadsheet.

2.4. Impedance Spectroscopy: Preliminaries

The impedance response, $Z(\omega)$, of the specimen can be written in complex form as,

$$Z(\omega) = Z'(\omega) - iZ''(\omega) \quad (1)$$

where $Z'(\omega)$ is the resistive (real) component, $Z''(\omega)$ is the reactive (imaginary) component and $i = \sqrt{-1}$. When a concrete specimen placed between a pair of electrodes and then subjected the action of a small amplitude alternating electrical current over a frequency range extending several decades, the specimen will exhibit an impedance response as shown in Figure 3. In this Figure, the frequency increases from right to left across the plot. The impedance response comprises two distinct features,

(i) a low-frequency spur associated with the polarization at the interface between the electrodes and the specimen [40-42]. The spur represents a portion of a much larger arc which would only become evident at considerably low frequencies (e.g. $\ll 1$ Hz); and,

(ii) a high-frequency arc with centre depressed from the real axis representing the bulk response of the material [43, 44].

The true bulk resistance of the test specimen, R (Ω), can be obtained from the intercept of the low-frequency end of the arc with the real axis (cusp point) as indicated. The bulk resistivity of the material, ρ, can then be calculated for a prismatic specimen by the relationship,

$$\rho = R\frac{A}{L} \ \ \Omega\text{-m} \tag{2}$$

where A is the cross-sectional area of the test specimen (m^2) and L is the distance between the electrodes (m), with $\frac{A}{L}$ giving the geometrical constant (m).

3. Test Results and Discussion

3.1 Influence of specimen size and contacting medium

Figures 4(a)–(c) present the Nyquist plots for all the four specimen dimensions obtained at 35 days curing. External electrodes were used in conjunction with the three different contacting media: conductive gel, sponges saturated with $Ca(OH)_2$ and sponges saturated using tap-

water. In these figures, frequency increases from right to left and, purely for reasons of clarity, only every 20th data marker has been highlighted to indicate the response per decade. These figures show that each specimen exhibits a similar overall response, comprising a spur at the low-frequency end which replicates the schematic shown in Figure 3, and two semicircular arcs which develop over intermediate and high frequency ranges. The intermediate arc is a feature typical of cement-based systems in which the measurement is taken using two external plate electrodes and saturated sponges as the contact medium between the electrode and test specimen [26]. The high-frequency arc represents the bulk response of the test specimen, which can be seen in most hardened cementitious materials as presented in the schematic in Figure 3.

The Nyquist plots presented in Figures 4(a)–(c) show that the specimen size has a strong influence on the specimen impedance across the entire frequency range, with the impedance increasing as specimen size decreases. This manifests itself as a progressive displacement of the Nyquist plot to the right-hand side, along with an increase in the diameter of the two semicircular arcs and in the prominence of the low-frequency spur. The decrease in impedance with increasing specimen size is a geometrical effect and is related primarily to the increase in the geometrical constant, A/L, as the specimen size increases. This effect is highlighted in Figure 4(d) whereby both $Z'(\omega)$ and $Z''(\omega)$ in Figure 4(c) are multiplied by the respective geometric constant [i.e. 0.045, 0.064, 0.094 and 0.144 m for, respectively, the 50, 70, 100 and 150 mm^2 cuboidal specimens, where the thickness of the sponges has been considered in the evaluation of L]. This geometric correction is shown to remove the considerable variations in the measured response and produces a much more uniform response, although some differences are still observable at the right-hand side of the plots, especially with regard to the low-frequency spur. This could be, in part, attributed to the

increasing influence of the electrode polarization with decreasing contact area, *A*, and the polarization at the specimen/contacting medium interface discussed below.

With reference to the schematic in Figure 5, Table 6 provides the summary of the frequency values at the junction between the right-hand electrode spur and the mid-frequency arc of the impedance spectra shown in Figures 4(a)–(c) (referred to as the low-frequency cusp point, $f_{c,l}$) and the values at the junction between the high- and mid- frequency arcs (the high-frequency cusp point, $f_{c,h}$), along with the frequencies at which the two bulk arcs maximize (referred to, respectively, as the mid-frequency peak point, $f_{p,m}$, and the high-frequency peak point, $f_{p,h}$). It is evident from Table 6 that both $f_{c,l}$ and $f_{p,m}$ are sensitive to the type of the specimen/electrode contacting medium, with the coefficient of variation (CoV) in $f_{c,l}$ decreasing with increasing specimen size and with the CoV in $f_{p,m}$ displaying an opposite trend. This is due to the decreasing influence of electrode/specimen interfacial polarization with increasing specimen size. Regardless of the type of the contacting medium, the results presented in Table 6 clearly highlight the specimen-size dependency of $f_{c,l}$, $f_{p,m}$ and $f_{c,h}$ over the range of specimen size considered, with the frequency generally decreasing with increasing specimen size. It is also interesting to note that $f_{p,h}$ is virtually independent of specimen size and contacting medium, indicating that $f_{p,h}$ is related to the bulk properties of the material itself and could, potentially, be utilized as a parameter in the characterization of the cement-paste microstructure.

On closer examination of the individual Nyquist plots presented in Figures 4(a)–(c), it is apparent that the contacting medium has an important role to play in determining the magnitude of the impedance across the entire frequency range. To better highlight the influence of contacting medium, the impedance spectra are replotted in Figures 6(a)–(d) in

terms of individual specimen size. It is evident from these Figures that the high-frequency (bulk) arc obtained using conductive gel and that obtained using sponges saturated with $Ca(OH)_2$ is very similar, with the latter showing only a slight increase in diameter, while the differences at the mid-frequency (secondary) arcs are quite prominent. The same tendency can also be seen in the low-frequency spur. This would indicate that the contacting medium has more of an influence at the low-frequency end of the response, although its effect is present over the entire frequency range; however, the overall trend is that its influence diminishes rapidly with increasing frequency.

The role of the contacting medium can be better understood from the results obtained using tap-water saturated sponges which were more resistive. It is apparent Figures 6(a)–(d) that increasing the resistance of the contacting medium results in the entire spectrum moving to the right and the two arcs and the spur increasing in size, with the shift/increase being more prominent in the low-frequency (right-hand) side of each curve, which corroborates earlier findings. It is also apparent that the measured resistance at the high-frequency cusp point varies, which indicates the residual influence of the contacting medium even at this high frequency range (see $f_{c,h}$ in Table 6). If the resistance of the contacting medium can be determined, it should then be possible to calculate the true bulk resistance (hence resistivity/conductivity) of the ECC specimens.

To develop this concept, impedance measurements were taken with only the contacting medium placed between the electrodes, with measurements taken immediately after the measurement of each individual test specimen. The results from this series of tests are presented in Figures 7(a)–(d), again, only every 20^{th} data marker is highlighted to indicate the response per decade. It is worth noting that these measurements were undertaken using the

same test setup: viz. the same electrodes, sponges and mass, but with the test specimen now being placed above the upper electrode along with the mass (see Section 2.3). It is evident from these Figures that the sponges saturated with tap-water exhibit a typical impedance response of a porous material comprising a low-frequency spur and a semicircular arc, which are not dissimilar to the schematic shown in Figure 3. The arc intercepts the real axis in the frequency range 5.5–12.5kHz at a resistance value of 219 Ω, 106.9 Ω, 61.4 Ω and 31.9 Ω for, respectively, the 50, 70, 100 and 150 mm square sponge; this gives the bulk resistance of the (two) tap-water saturated sponges. As the impedance of the contacting medium decreases, this is seen to result in an almost linear impedance response which, for the $Ca(OH)_2$ saturated sponges, intercepts the real axis in the frequency range 30-100kHz at 29.7 Ω, 15.2 Ω, 8.1 Ω, and 4.6 Ω with increasing sponge size from, respectively, 50mm to 150mm. For the conductive gel, the intercept lies within a much narrower range (1-1.5 Ω) with a corresponding cusp-point frequency ranging from 25-65kHz for the four different specimen dimensions. It is now possible to calculate the bulk resistance of the ECC specimens, R_{ECC}, by subtracting the resistance of the contacting medium, R_{cont}, obtained as above from the measured resistance of the specimens, $R_{ECC+cont}$, which included the contacting medium,

$$R_{ECC} = R_{ECC+cont} - R_{cont} \tag{3}$$

In equation (3), $R_{ECC+cont}$ is obtained from the intercept of the low-frequency end of the bulk arc with the real axis following the schematic presented in Figure 8 through the equation,

$$R_{ECC+cont} = Z'_{c,h} + \frac{{Z''_{c,h}}^2}{Z'_{c,h}} = \frac{{Z'_{c,h}}^2 + {Z''_{c,h}}^2}{Z'_{c,h}} \tag{4}$$

where $Z'_{c,h}$ and $Z''_{c,h}$ are, respectively, the measured resistive and reactive components of the impedance as per equation (1) at the high-frequency cusp point (i.e. $\omega = \omega_{c,h}$). The bulk resistivity can thus be evaluated by substituting equation (4) into equations (3) and then (2).

The bulk resistivity values obtained by following the above procedure are presented in Figures 10(a) and (b), with the results displayed in Figure 10(a) computed directly from the bulk resistance of each individual specimen using equations (2) and (4) and those presented in Figure 10(b) had the influence of the contacting medium removed using equation (3). An example of the input values used in the calculation of the bulk resistivity are presented in Table 7. Also presented in Figures 10(a) and (b) is the mean bulk resistivity values obtained at 28 days of curing using two types of contacting media: conductive gel and tap-water saturated sponges. In this series of measurements, the impedance of the sponges was measured twice to check the influence of specimen weight: ms-series representing measurements with both the specimen and the mass placed on the upper electrode (similar to the procedure adopted at 35 days of curing) and m-series, with only the mass placed on the upper electrode. For benchmarking purposes, all the computed bulk resistivity values obtained above are compared with the values obtained from the prismatic (i.e. 40×40×160mm) ECC specimens using internal (embedded)-plate electrodes in which the Nyquist plots are displayed in Figure 9. For each cube size, the measurements at the 28-day were undertaken on all three notionally identical specimens and error bars representing ± one standard deviation have been included in Figure 10(a) to highlight the variation between the specimens. It was found that the coefficient of variations computed from the bulk resistivity of replicate specimens were within 5%, indicating good repeatability. Measurements at 35-day were only undertaken on one representative cube from each size and results should be considered with this in mind.

Taking the bulk resistivity obtained from the prismatic specimens as the *true* bulk resistivity of the material (as there is no interference from the contacting medium), it can be inferred from Figure 10(a) that the computed bulk resistivity obtained from the external-plate

electrodes consistently overestimates the actual bulk resistivity of the ECC and is affected significantly by the type of the contacting media. The general trend is that the computed resistivity obtained through tap-water-saturated sponges decreases with increasing specimen size, while those obtained through either conductive gel or $Ca(OH)_2$-saturated sponges shows the opposite trend. Once the contacting medium effects have been removed (see Figure 10(b) and Table 7), the bulk resistivity values are now in good agreement, with the lines connecting the data points superimposed on each other. On closer examination, however, it is apparent that the bulk resistivity of the larger specimens is higher than those of the smaller specimens and specimens with measurements taken with internal (embedded)-plate electrodes, indicating the existence of *size effect*. Considering the key parameters affecting the bulk resistivity of cementitious materials in general [45], it could be expected that for the curing condition employed in the present study, there were no appreciable differences in the degree of hydration and the degree of pore saturation resulting from self-desiccation. A possible reason for the apparent size dependency may be attributed to a geometrical effect (i.e. the relative size of the fibers in relation to size of the specimen). Despite the fact that PVA fibers are hydrophilic, it has been shown that their presence in the ECC matrix increases the porosity of the matrix at the transition zone around the fibers [46] which, from an electrical point of view, could be expected to modify the continuity and tortuosity of the pore system. It is postulated that as the size of the specimen decreases, this leads to a less tortuous conduction path through the specimen, hence a lower apparent bulk resistivity. However, this feature warrants further investigation.

3.2 Origins of the mid-frequency arc

To correct for the influence of electrode effects, the impedance of the contacting medium was *subtracted* from the measured impedance of the ECC cube, which included the contacting

medium, over the entire frequency range. For illustrative purposes, the resulting synthesized Nyquist plots for 150mm cuboidal specimen are displayed in Figures 11(a) and (b). It is evident that the synthesized high-frequency (bulk) arcs is insensitive to the contacting medium, indicating a *true* representation of the bulk response of the ECC. While some minor differences are still present, the similarity in the high-frequency arc corroborates the applicability of equation (3) at frequencies higher than that of the high-frequency cusp-point ($f_{c,h}$). At lower frequencies, however, considerable variations exist and related to the type of contacting medium used in the measurement. Given that the equation (3) fails to remove the mid-frequency arc, this feature must originate from another mechanism(s) operative within this frequency region. It is postulated that the emergence of the mid-frequency arc is related to polarization processes operative at the specimen/contacting medium interface (see Figure 12) for example, a solid/liquid interfacial process [47, 48]. The presence of the small spur on the right-hand side of each curve indicates the residual polarization at the electrode/contacting medium interface.

3.3 Influence of the quality of contact surface

Given that the mid-frequency arc discussed above has a direct link with the contacting medium/specimen interface, the *quality* of the contact surface between the specimen and the contacting medium could also influence electrical properties. To study this effect, Figures 13(a)–(d) present the Nyquist plots for 150mm and 100mm cuboidal specimens, with measurements on each specimen taken on three pairs of opposing surfaces denoted 1-1' and 2-2' representing two pairs of the side surfaces (surfaces cast against the steel mold) and 3-3' representing the bottom and top (as cast) surfaces; the definition and photos of each surface pair are displayed in Figure 14. As before, electrical measurements were taken using

external-plate electrodes and two different contacting media: conductive gel and tap-water-saturated sponges.

Consider, for example, the response of 100mm cube presented in Figure 13(c). Despite the similarity in the size of the primary bulk arc, it is apparent that the size of the secondary arc varies considerably and is sensitive to which pair of opposing surface the measurement was taken. Most notable is the anomalously large secondary arc exhibited by surfaces 2-2' and 3-3', which is seen to cause the spur to displace to the right along the real axis. It is proposed that the origin of this feature is related to the presence of large surface voids (see the images of surface 2-2' of the 100mm specimen in Figure 14) and for surface 3-3', this is due to the presence of surface irregularities on the cast surface (surface 3'), both of which are shown to accentuate polarization at the specimen/contacting medium interface and hence the extent and prominence of the mid-frequency arc. The prominence of this arc is shown to be minimal and insensitive to the quality of the contact surface when conductive gel was used (see Figure 13(d)) as in this instance the gel provided the opportunity to fill the large surface voids manually as the 2mm thick contacting surface was created. The mid-frequency arc is, however, still present due to the specimen/contacting medium interface as discussed earlier.

Despite the significant variations in the size of the secondary arc, it is interesting to note from the plots presented in Figures 13(a)–(d) that the bulk (primary) arcs are similar regardless of which pair of opposing surface the measurement was taken. These arcs represent the bulk response of the system (i.e. test specimen and contacting medium combined together) and equation (3) could be used to correct for the influence of contacting medium; as such, the bulk response of the test specimen itself could be obtained (see Section 3.2).

With reference to Figures 13(a)–(d), although the quality of the contact surface and the type of contacting medium have negligible influence on the bulk response, they have a considerable influence at lower frequencies (i.e. at frequencies lower than the high-frequency cusp point). This is particularly relevant when taking repeated measurements over an extended period of time, particularly when the test frequency employed is significantly lower than that of the high-frequency cusp point. As such, any measurement should be performed on the same pair of opposing faces to ensure consistency.

3.4 Influence of the moisture content of the contacting medium

To simulate possible variations in *squeezing quality* from different operators, an additional four tests were taken on the 150mm cuboidal specimen at 31 days after casting using sponges with varying moisture contents. In this series, only tap-water saturated sponges were used as this was shown to accentuate the impedance response. In the first measurement, saturated sponges were used following the procedure detailed in Section 2.3, while in the rest of the measurements, the sponges were made partially saturated by squeezing them manually by hand. As such, the sponges were always in a drier state with the order of the measurement. Before squeezing the sponges, additional sweep frequency measurement was taken immediately after measuring the impedance of the specimen, with only the sponges placed between the two electrodes. During this measurement, the specimen was returned to the curing tank to negate any drying effect. Once the measurement of the sponges was completed, the specimen was removed from the tank and the surface was then surface-dried with a paper towel.

The Nyquist plots for the 150mm specimen with measurements taken using tap-water sponges with varying degrees of saturation are displayed in Figure 15(a), with the response of

the sponges used in each individual test presented in Figure 15(b). It is evident from Figure 15(a) that the impedance plots exhibit similar features to that shown previously in Figure 7(a) regardless of the degree of saturation of the sponges. It is apparent as the degree of saturation of the sponges decreases (i.e. sponge gets drier), their impedance increases (see Figure 15(b)), resulting into a displacement of the respective plot in Figure 15(a) to the right which indicates an overall increase in impedance. It is also apparent that the influence arising from the sponges is present over the entire frequency range, although its prominence diminishes rapidly with increasing frequency.

To explore whether equation (3) is still applicable, the same calculation as implemented in Section 3.1 was repeated and the results are summarized in Table 8, together with the corresponding value obtained from the prismatic specimen with embedded electrodes for benchmarking purposes. This Table shows that the bulk resistivity values obtained from the subtraction method are in good agreement and comparable to that of the prism, within a ±10% scatter. On closer examination, however, it is evident that the computed bulk resistivity from the two-point measurement using external-plate electrodes decreases with increasing resistance of the contacting medium (or with decreasing degrees of saturation). The exact reason behind this phenomenon is not known and forms a scope for further investigation; suffice to state here that the proposed work has shown a potential way forward to obtain the bulk resistivity of the material, with further challenges remaining to improve its accuracy.

4. Conclusions

This present work had, as its goal, a fundamental understanding of the influence of specimen size, contacting medium, quality of the contacting surface and degree of saturation of the contacting sponge on the complex impedance of an engineered cementitious composite.

These factors, ultimately, will influence measurement protocols. The following conclusions can be drawn from the work presented:

1. It is shown that as specimen size increases, its impedance across the entire frequency range decreases and is, in part, attributed to the increase in the geometrical constant, *A/L*, with increasing specimen size.
2. The use of a contacting medium in the *end-to-end* two-point technique is shown to introduce a spurious response which is detectable across the entire frequency range. This specifically results into the development of an intermediate arc in the Nyquist plot which originates from the polarization at the specimen/contacting medium interface. This arc is present over the frequency range ~50Hz to ~100kHz yet is not seen in the impedance response of specimens with embedded electrodes. The prominence of this arc is dependent upon the impedance of the contacting medium, the quality of the contacting surface and curing time.
3. The intermediate arc is shown to be sensitive to which pair of opposing surfaces the measurement is taken. An anomalously large intermediate arc is seen in specimens with large surface voids or surface irregularities. This could be particularly relevant when taking repeated measurements on a cuboidal-shape specimen over an extended period of time, especially when the test frequency employed is significantly lower than that of the high-frequency cusp point. In this instance, any measurement should be performed on the same pair of opposing surfaces to ensure consistency.
4. The bulk resistance of the ECC could be obtained by a simple subtraction method using equation (3). It is shown that this method is applicable to a range of contacting media used in the present study, including conductive gel, synthetic sponges saturated with calcium hydroxide solution and similar sponges either fully or partially saturated with tap-water.

Acknowledgements

The authors wish to acknowledge the financial support of the Engineering and Physical Sciences Research Council (EPSRC) (Grant EP/N028597/1) and the generous support of Kuraray Japan and Kuraray Europe GmbH for providing the PVA fibers and BASF UK for providing the admixtures. DS and HMT also wish to acknowledge the financial support provided by Heriot-Watt University.

References

[1] V.C. Li, Engineered cementitious composites (ECC): material, structural, and durability performance, in: E.G. Nawy (Ed.), Concrete Construction Engineering Handbook, CRC Press, Boca Raton, United States of America, 2008, pp. 24-1–46. DOI: 10.1201/9781420007657.ch24

[2] M.D. Lepech, V.C. Li, Water permeability of engineered cementitious composites, Cem. Concr. Compos. 31 (10) (2009) 744–753. DOI: 10.1016/j.cemconcomp.2009.07.002

[3] M. Li, V.C. Li, Cracking and healing of engineered cementitious composites under chloride Environment, ACI Mater. J. 108 (3) (2011), 333–340. DOI: 10.14359/51682499

[4] S. Qian, J. Zhou, M.R. de Rooij, E. Schlangen, G. Ye, K. van Breugel, Self-healing behavior of strain hardening cementitious composites incorporating local waste materials, Cem. Concr. Compos. 31 (9) (2009) 613–621. DOI: 10.1016/j.cemconcomp.2009.03.003

[5] B. Suryanto, S.A. Wilson, W.J. McCarter, T.M. Chrisp, Self-healing performance of engineered cementitious composites under natural environmental exposure, Adv. Cem. Res. 28 (4) (2016) 211–220. DOI: 10.1680/adcr.15.00022

[6] K. Kobayashi, D. Le Ahn, K. Rokugo, Effects of crack properties and water-cement ratio on the chloride proofing performance of cracked SHCC suffering from chloride attack, Cem. Concr. Compos. 69 (2016) 18–27. DOI: 10.1016/j.cemconcomp.2016.03.002

[7] H. Liu, Q. Zhang, C. Gu, H. Su, V.C. Li, Influence of micro-cracking on the permeability of engineered cementitious composites, Cem. Concr. Compos. 72 (2016) 104–113. DOI: 10.1016/j.cemconcomp.2016.05.016

[8] M. Şahmaran, V.C. Li, Influence of microcracking on water absorption and sorptivity of ECC, Mater. Struct. 42 (5) (2009) 593–603. DOI: 10.1617/s11527-008-9406-6

[9] S.C. Paul, G.P. van Zijl, A.J. Babafemi, M.J. Tan, Chloride ingress in cracked and uncracked SHCC under cyclic wetting-drying exposure, Construct. Build. Mater. 114 (2016) 232–240. DOI: 10.1016/j.conbuildmat.2016.03.206

[10] W.J. McCarter, B. Suryanto, H.M. Taha, S.V. Nanukuttan, P.A.M. Basheer, A testing methodology for performance-based specification, J. Struct. Integrity Maint. 2 (2) (2017) 78–88. DOI: 10.1080/24705314.2017.1318040

[11] C. Gehlen, H.M. Ludwig, Compliance testing for probabilistic design purposes: probabilistic performance based durability design of concrete structures, DuraCrete EU-Brite EuRam III, Document BE95-1347/R8, March 1999.

[12] W.J. McCarter, G. Starrs, A. Adamson, T.M. Chrisp, P.A.M. Basheer, S.V. Nanukuttan, S. Srinivansan , C. Green, Influence of different European cements on the hydration of cover-zone concrete during the curing and postcuring periods, J Mater. Civil Eng. 25 (9) (2012) 1335–1343. DOI: 10.1061/(ASCE)MT.1943-5533.0000678

[13] W.J. McCarter, T.M. Chrisp, G. Starrs, A. Adamson, P.A.M. Basheer, S.V. Nanukuttan, S. Srinivasan, C. Green, Characterization of physio-chemical processes and hydration kinetics in concretes containing supplementary cementitious materials using electrical

property measurements, Cem. Concr. Res. 50 (2013) 26–33. DOI: 10.1016/j.cemconres.2013.03.008

[14] W.J. McCarter, T.M. Chrisp, G. Starrs, E.H. Owens, Setting, hardening and moisture-loss within a cement-based backfill grout under simulated repository environments, Measurement 45 (3) (2012) 235–242. DOI: 10.1016/j.measurement.2011.12.014

[15] J. Castro, R. Spragg, P. Kompare, W.J. Weiss, Portland cement concrete pavement permeability performance, Technical Report Joint Transportation Research Program Indiana Department of Transportation and Purdue University Publication FHWA/IN/JTRP-2010/29, November 2010, http://docs.lib.purdue.edu/cgi/viewcontent.cgi?article=2592&context=jtrp.

[16] W.J. McCarter, G. Starrs, T.M. Chrisp, P.A.M. Basheer, S.V. Nanukuttan, S. Srinivasan, Conductivity/activation energy relationships for cement-based materials undergoing cyclic thermal excursions, J. Mater. Sci. 50 (3) (2015) 1129–1140. DOI: 10.1007/s10853-014-8669-2

[17] B. Suryanto, W.J. McCarter, G. Starrs, G.V. Ludford-Jones, Electrochemical immittance spectroscopy applied to a hybrid PVA/steel fiber engineered cementitious composite, Mater. Design 105 (2016) 179–189. DOI: 10.1016/j.matdes.2016.05.037

[18] K. Kurumisawa, T. Nawa, Electrical conductivity and chloride ingress in hardened cement paste, J. Adv. Concr. Tech. 14 (3) (2016) 87–94. DOI: 10.3151/jact.14.87

[19] M.D. Newlands, M.R. Jones, S. Kandasami, T.A. Harrison, Sensitivity of electrode contact solutions and contact pressure in assessing electrical resistivity of concrete, Mater. Struct. 41 (4) (2008) 621–632. DOI: 10.1617/s11527-007-9257-6

[20] R.P. Spragg, J. Castro, T. Nantung, M. Paredes, W.J. Weiss, Variability analysis of the bulk resistivity measured using concrete cylinders, Adv. Civ. Eng. Mater. 1 (1) (2012) 1–17. DOI: 10.1520/ACEM104596

[21] O. Sengul, Use of electrical resistivity as an indicator for durability, Constr. Build. Mater. 73 (2014) 434–441. DOI: 10.1016/j.conbuildmat.2014.09.077

[22] H. Layssi, P. Ghods, A.R. Alizadeh, M. Salehi, Electrical resistivity of concrete, Concr. Inter. 37 (5) (2015) 41–46.

[23] P. Ghosh, Q. Tran, Correlation between bulk and surface resistivity of concrete, Int. J. Concr. Struct. M. 9 (1) (2015) 119–132. DOI: 10.1007/s40069-014-0094-z

[24] J. Gudimettla, G. Crawford, Resistivity tests for concrete–recent field experience, ACI Mater. J. 113 (4) (2016), 505–512. DOI: 10.14359/51688830

[25] W.J. McCarter, G. Starrs, S. Kandasami, M.R. Jones, T.M. Chrisp, Electrode configurations for resistivity measurements on concrete, ACI Mater. J. 106 (3) (2009) 258–264. DOI: 10.14359/56550

[26] W.J. McCarter, H.M. Taha, B. Suryanto, G. Starrs, Two-point concrete resistivity measurements: interfacial phenomena at the electrode–concrete contact zone, Meas. Sci. Technol. 26 (8) (2015) 085007. DOI: 10.1088/0957-0233/26/8/085007

[27] W.J. McCarter, T.M. Chrisp, A. Butler, P.A.M. Basheer, Near–surface sensors for condition monitoring of cover-zone concrete, Constr. Build. Mater. 15 (2) (2001) 115–124. DOI: 10.1016/S0950-0618(00)00060-X

[28] W.J. McCarter, T.M. Chrisp, G. Starrs, A. Adamson, E. Owens, P.A.M. Basheer, S.V. Nanukuttan, S. Srinivasan, N. Holmes, Developments in performance monitoring of concrete exposed to extreme environments, ASCE J. Infrastruct. Syst. 18 (3) (2011) 167–175. DOI: 10.1061/(asce)is.1943-555x.0000089

[29] M. Hallaji, A. Seppänen, M. Pour-Ghaz, Electrical resistance tomography to monitor unsaturated moisture flow in cementitious materials, Cem. Concr. Res. 69 (2015) 10–18. DOI: 10.1016/j.cemconres.2014.11.007

[30] B. Suryanto, D. Saraireh, J. Kim, W.J. McCarter, G. Starrs, H.M. Taha, Imaging water ingress into concrete using electrical resistance tomography, Int. J. Adv. Eng. Sci. Appl. 9 (2) (2017) 109–118. DOI: 10.1007/s12572-017-0190-9

[31] British Standards Institution, BS EN12390-1: 2012, Testing hardened concrete – Part 1: shape, dimensions and other requirements for specimens and moulds, BSI, London, 2012. DOI:10.3403/30254400.

[32] American Concrete Institute, ACI 318M-14, Building code requirements for structural concrete (ACI 318M-14) and Commentary (ACI 318RM-14), ACI, Farmington Hills, 2015.

[33] American Society for Testing and Materials International, ASTM C31/C31M–17, Standard practice for making and curing concrete test specimens in the field, ASTM International, West Conshohocken, 2017. DOI: 10.1520/C0031_C0031M-17.

[34] Japan Society of Civil Engineers, Concrete Engineering Series 82, Recommendations for Design and Construction of High Performance Fiber Reinforced Cement Composites with Multiple Fine Cracks (HPFRCC), JSCE, 2008. https://www.jsce.or.jp/committee/concrete/e/hpfrcc_JSCE.pdf

[35] Canadian Standards Association, CSA A23.1-14/A23.2-14, Concrete materials and methods of concrete construction (CSA A23.1) and Test methods and standard practices for concrete (CSA A23.2), CSA, Mississauga, 2014.

[36] P. Langford, J.P. Broomfield, Monitoring the corrosion of reinforcing steel, *Construct. Repair*, 1 (2) (1987), 32–36.

[37] J.P. Broomfield. Corrosion of Steel in Concrete, first ed., E&FN Spon, London, 1997 (ISBN 0 419 19630 7).

[38] K. Osterminski, R.B. Polder, P. Schiessl, Long term behaviour of the resistivity of concrete, Heron 57 (3) (2012) 211–230. UUID:c77effc5-c5bd-46db-813e-bcc4fb5efa54

[39] British Standards Institution, BS EN 197-1:2011—Cement: Composition, Specifications and Conformity Criteria for Common Cements, BSI, London, 2000.

[40] W.J. McCarter, S. Garvin, N. Bouzid, Impedance measurements on cement paste, J. Mater. Sci. Lett. 7 (10) (1988) 1056–1057. DOI: 10.1007/BF00720825

[41] P.B. Ishai, M.S. Talary, A. Caduff, E. Levy, Y. Feldman, Electrode polarization in dielectric measurements: a review, Meas. Sci. Technol. 24 (10) (2013) 102001. DOI: 10.1088/0957-0233/24/10/102001

[42] S.U.S. Lekshmi, P.N.V. Jayanthi, P. Aravind, D.N. Singh, M.S. Baghini, A critical analysis of the performance of plate- and point-electrodes for determination of electrical properties of the soil mass, Measurement 93 (2016) 552–562. DOI: 10.1016/j.measurement.2016.07.052.

[43] W.J. McCarter, R. Brousseau, The AC response of hardened cement paste, Cem. Concr. Res. 20 (6) (1990) 891–900. DOI: 10.1016/0008-8846(90)90051-X.

[44] W.J. McCarter, G. Starrs, T.M. Chrisp, Electrical monitoring methods in cement science, in: J. Bensted, P. Barnes (Eds.), Structure and Performance of Cements, Spon Press, London, United Kingdom, 2002, pp. 442–456. ISBN: 9780419233305

[45] W.J. McCarter, A. Butler, T.M. Chrisp, M. Emerson, G. Starrs, J. Blewett, Field trials on covercrete monitoring sensors, P. I. Civil Eng. Str. B. 146 (3), 295–305. DOI: 10.1680/stbu.2001.146.3.295.

[46] A.R. Sakulich, V.C. Li, Nanoscale characterization of engineered cementitious composites (ECC), Cem. Concr. Res. 41 (2) (2011) 169–175. DOI: 10.1016/j.cemconres.2010.11.001.

[47] M. Iwamoto, Maxwell–Wagner effect, in: B. Bhushan (Ed.), Encyclopedia of Nanotechnology, Springer Netherlands, 2016, pp. 1276–1285. DOI: 10.1007/978-90-481-9751-4_5.

[48] F. Galembeck, T.A.L. Burgo, Chemical Electrostatics–New Ideas on Electrostatic Charging: Mechanisms and Consequences, Springer International Publishing, Cham, Switzerland, 2017, pp. 38-48. DOI: 10.1007/978-3-319-52374-3.

Figure Captions

Figure 1. (a) Shematic of testing arrangement for *end-to-end* (two-point) measurements using external electrodes; and (b) experimental set-up for, respectively, 150mm, 100mm, 70mm and 50mm cubes.

Figure 2. (a) Shematic of testing arrangement for two-point measurements using embedded electrodes; and (b) experimental set-up.

Figure 3. Schematic showing the typical impedance response of a cementitious system.

Figure 4. (a) – (c) Influence of specimen size on the impedance response after 35 days curing; and (d) the response in (c) multiplied by the respective specimen geometrical constant, A/L.

Figure 5. Schematic showing salient frequencies on Nyquist plots.

Figure 6. Influence of contacting media on the impedance response of (a) 150mm cube; (b) 100mm cube; (c) 70mm cube; and (d) 50mm cube, with measuements taken at 35 days of curing.

Figure 7. Impedance response of the contacting media with varying cross-sectional area: (a) 150mm; (b) 100mm; (c) 70mm; and (d) 50mm.

Figure 8. Showing the definition of the intercept of the bulk arc with the real axis.

Figure 9. Impedance response of the prismatic specimens at 28- and 35- days of hydration.

Figure 10. Comparison of bulk resistivity obtained from the cuboidal specimens with varying specimen size and contacting medium to bulk resistivity obtained from 40×40×160 mm^3

prismatic specimens with embedded electrodes: (a) based on measured resistance; and (b) corrected data employing equation (3).

Figure 11. Sythesized Nyquist plots obtained by subtracting the Nyquist plots of the contacting medium from the Nyquist plot for the 150mm cuboidal specimen.

Figure 12. Idealized representation of interfacial polarization processes at the specimen/ electrode contact region under an imposed electrical field.

Figure 13. Variations in impedance response for each pair of surfaces for: (a) and (b) 150mm cube; and (c) and (d) 100mm cube.

Figure 14. Images of the test surfaces of 150mm and 100mm specimens.

Figure 15. (a) Influence of squeezing on the impedance response of 150mm cube; and (b) the corresponding impedance response of the sponges.

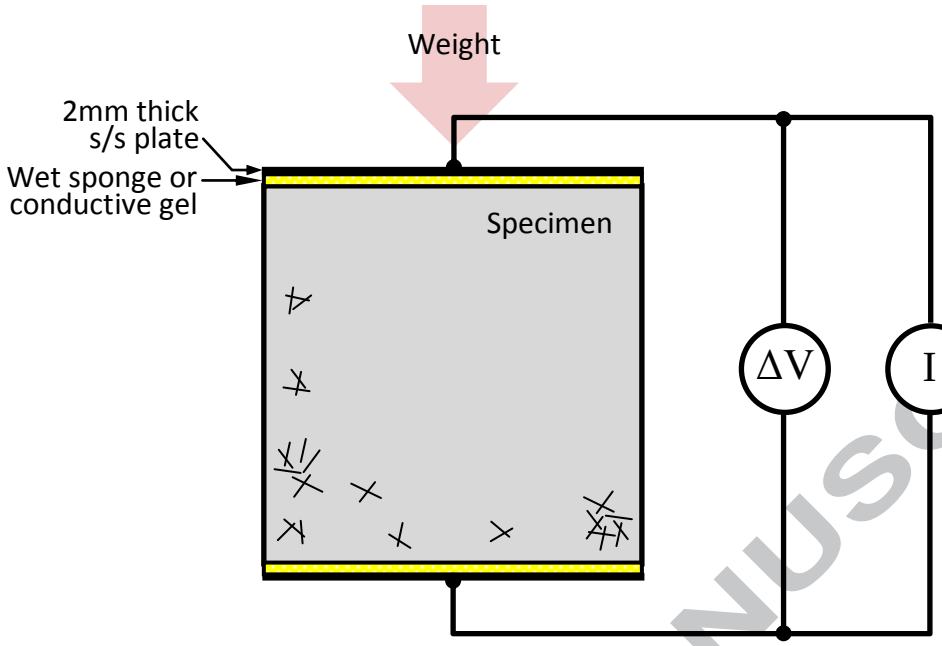

(a)

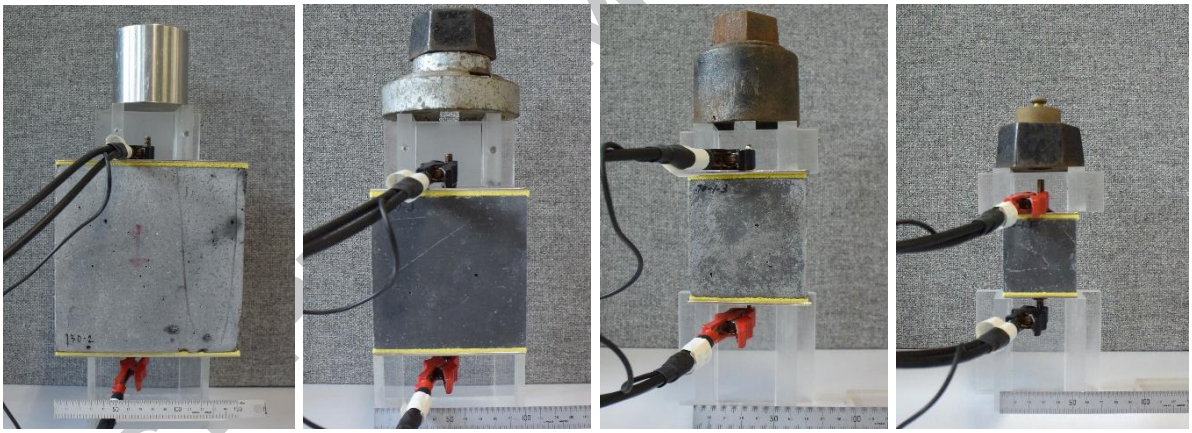

(b)

Figure 1. (a) Shematic of testing arrangement for *end-to-end* (two-point) measurements using external electrodes; and (b) experimental set-up for, respectively, 150mm, 100mm, 70mm and 50mm cubes.

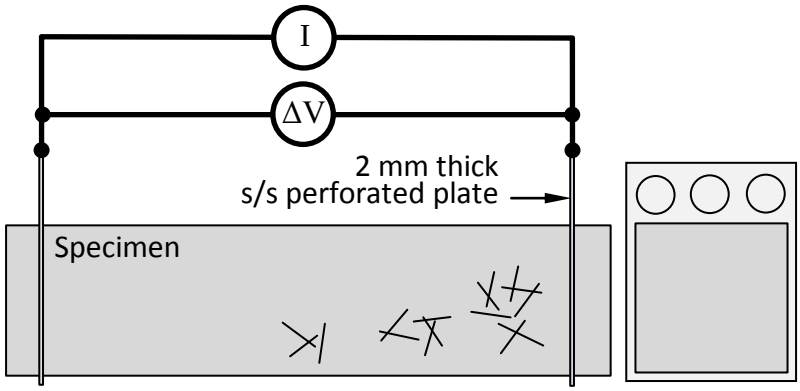

(a)

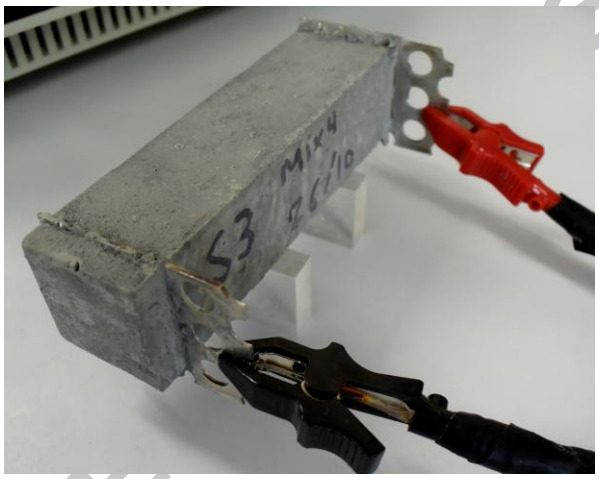

(b)

Figure 2. (a) Shematic of testing arrangement for two-point measurements using embedded electrodes; and (b) experimental set-up.

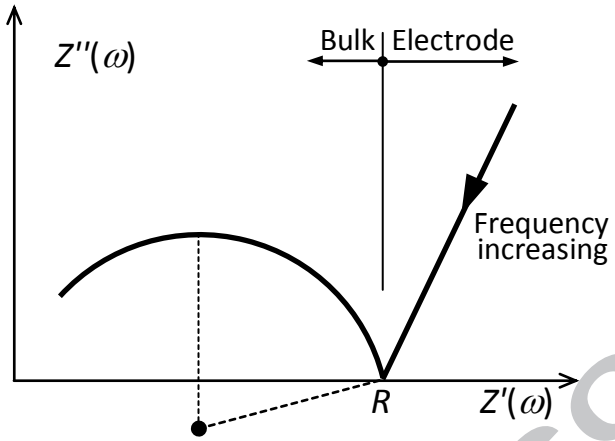

Figure 3. Schematic showing the typical impedance response of a cementitious system.

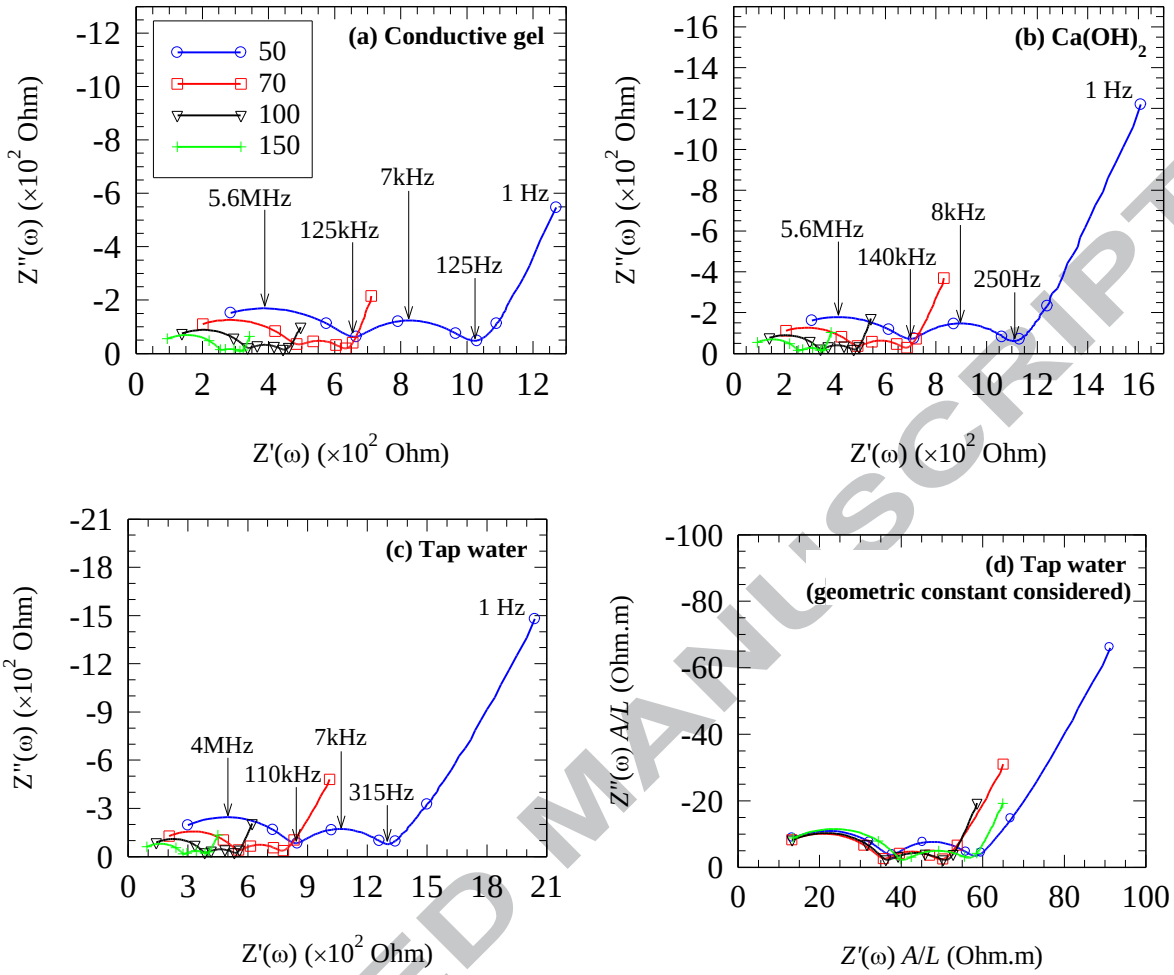

Figure 4. (a) – (c) Influence of specimen size on the impedance response after 35 days curing; and (d) the response in (c) multiplied by with the respective specimen geometrical constant, A/L.

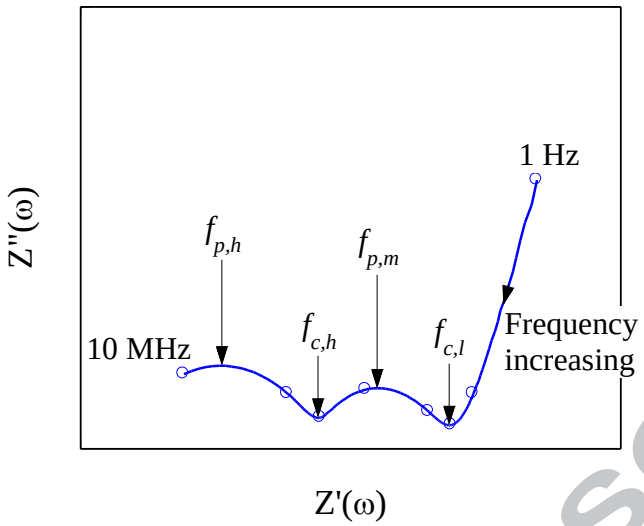

Figure 5. Schematic showing salient frequencies on Nyquist plots.

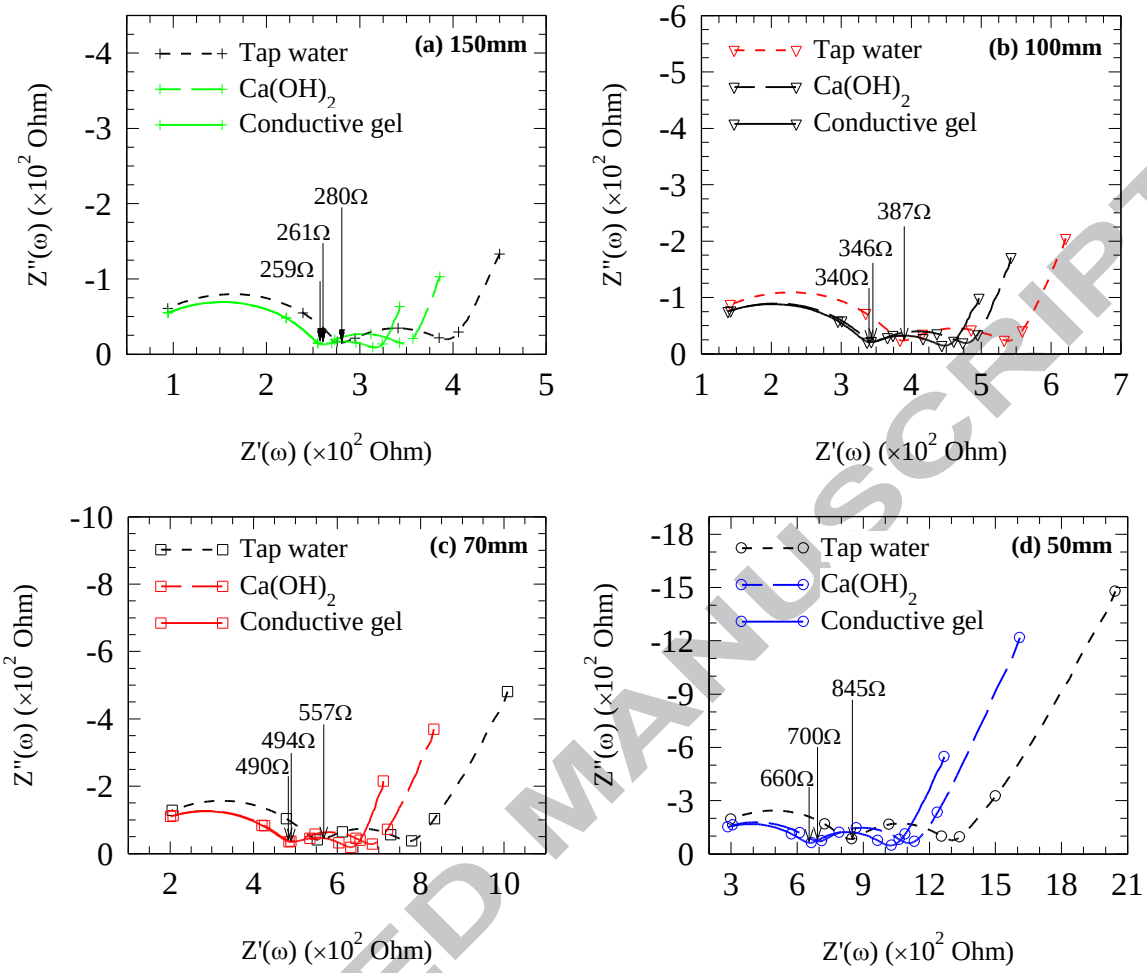

Figure 6. Influence of contacting media on the impedance response of (a) 150mm cube; (b) 100mm cube; (c) 70mm cube; and (d) 50mm cube, with measuements taken at 35 days of curing.

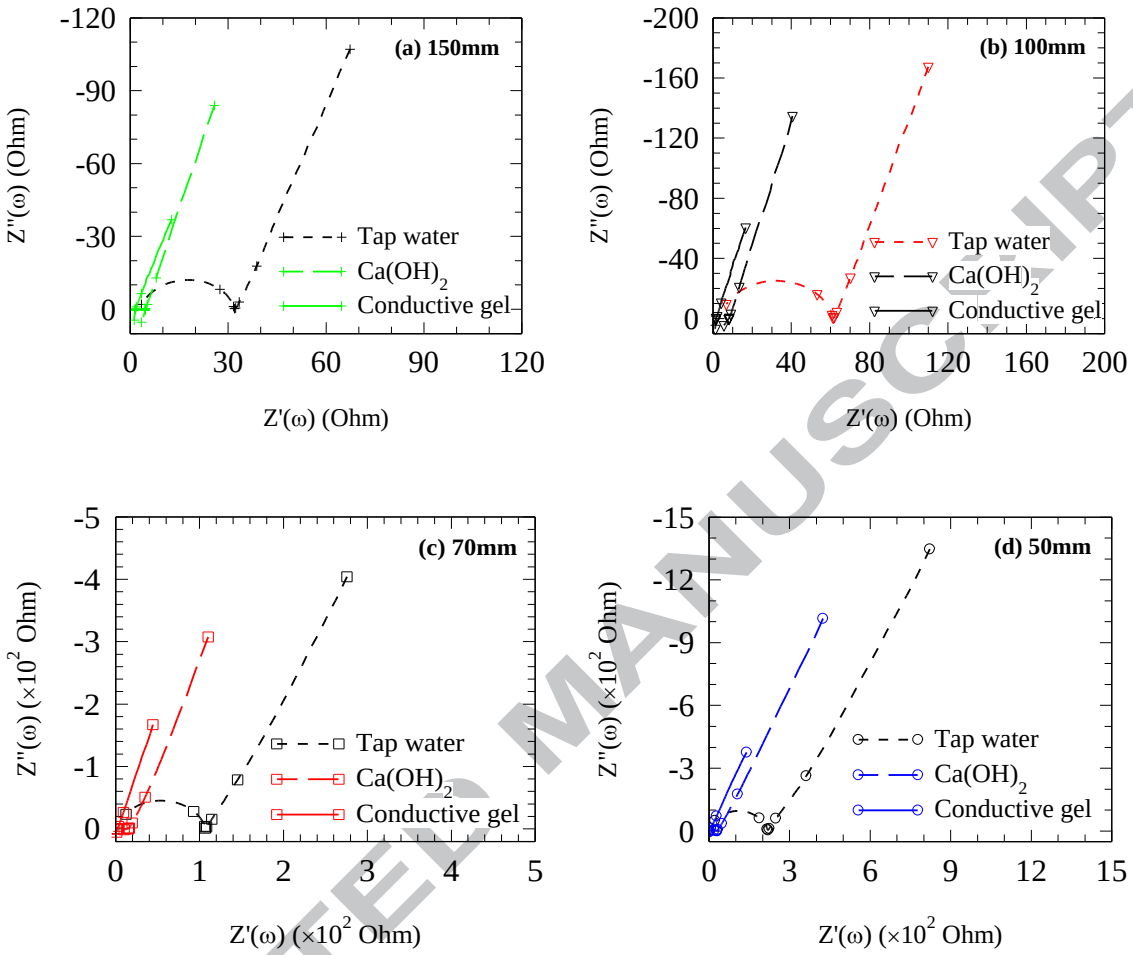

Figure 7. Impedance response of the contacting media with varying cross-sectional area: (a) 150mm; (b) 100mm; (c) 70mm; and (d) 50mm.

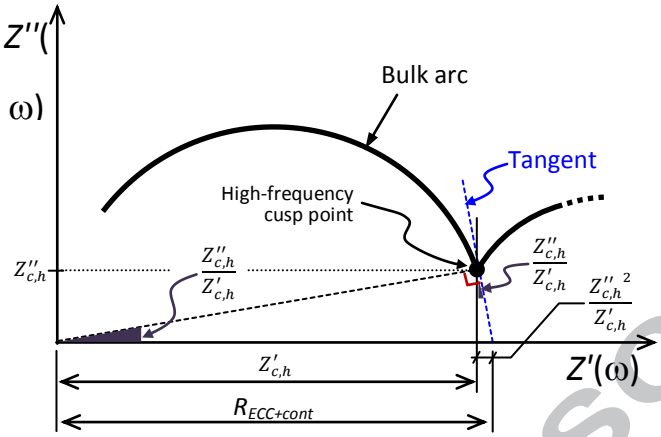

Figure 8. Showing the definition of the intercept of the bulk arc with the real axis.

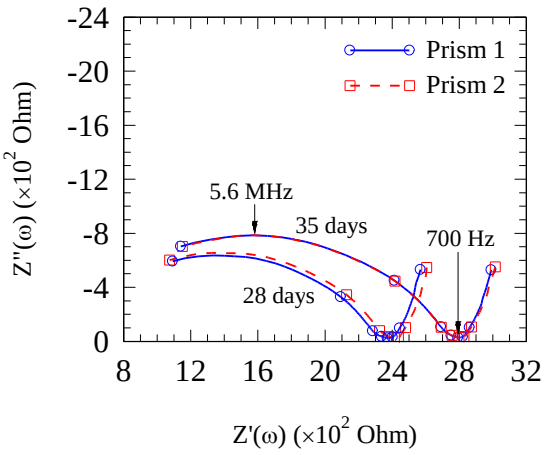

Figure 9. Impedance response of the prismatic specimens at 28 and 35 days of hydration.

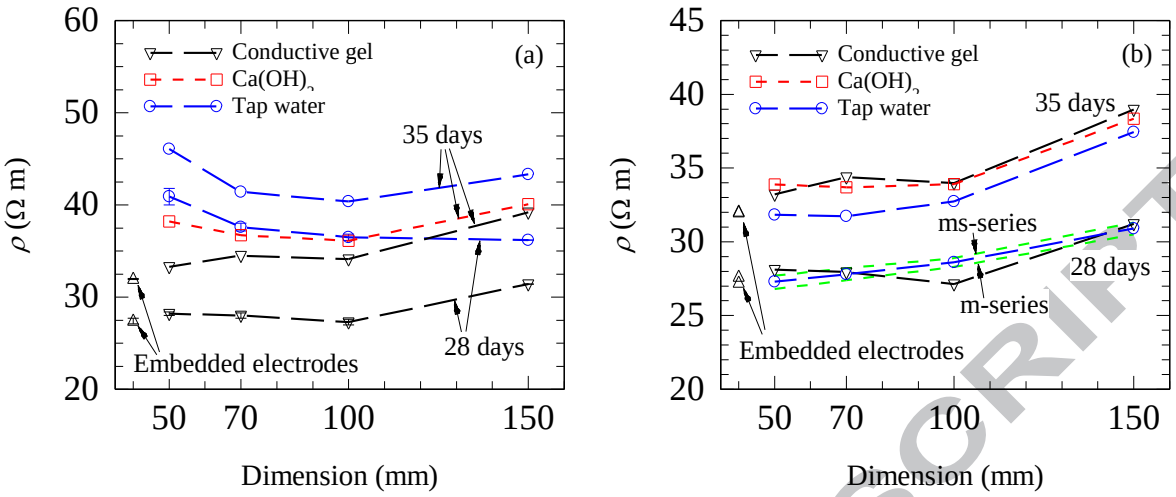

Figure 10. Comparison of bulk resistivity obtained from the cuboidal specimens with varying specimen size and contacting medium to bulk resistivity obtained from 40×40×160 mm^3 prismatic specimens with embedded electrodes: (a) based on measured resistance; and (b) corrected data employing equation (3).

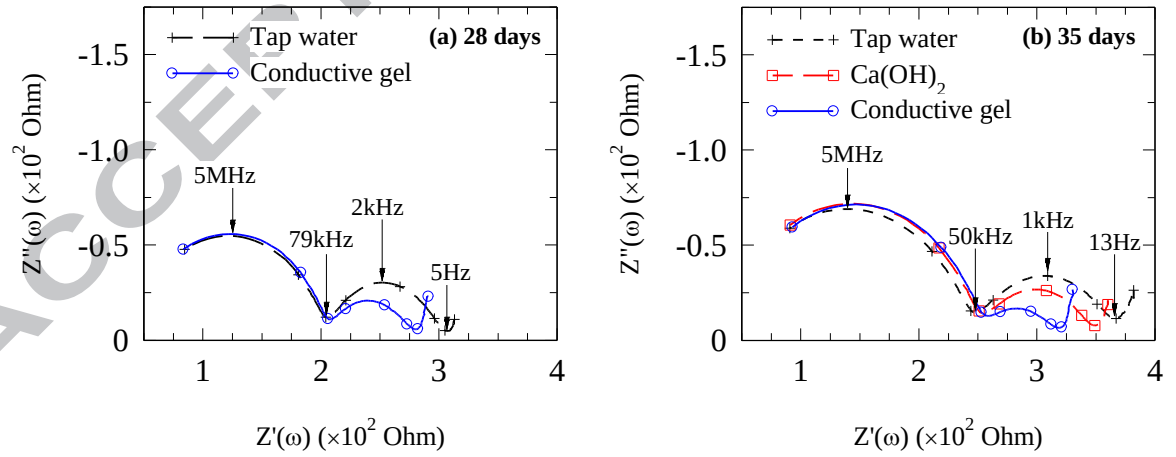

Figure 11. Sythesized Nyquist plots obtained by subtracting the Nyquist plots of the contacting medium from the Nyquist plot for the 150mm cuboidal specimen.

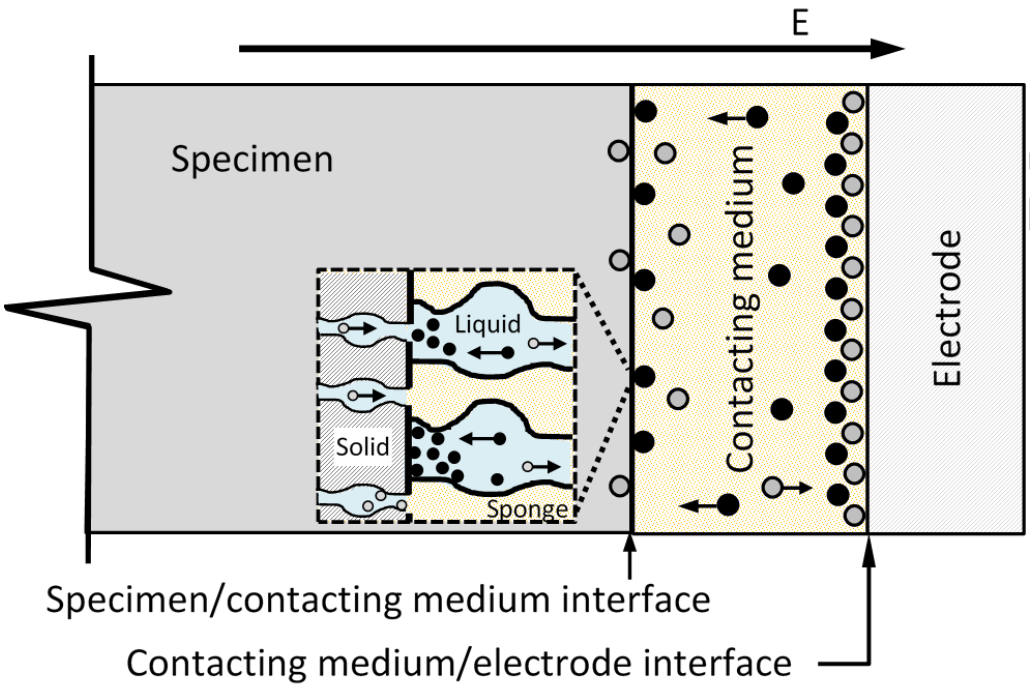

Figure 12. Idealized representation of interfacial polarization processes at the specimen/electrode contact region under an imposed electrical field.

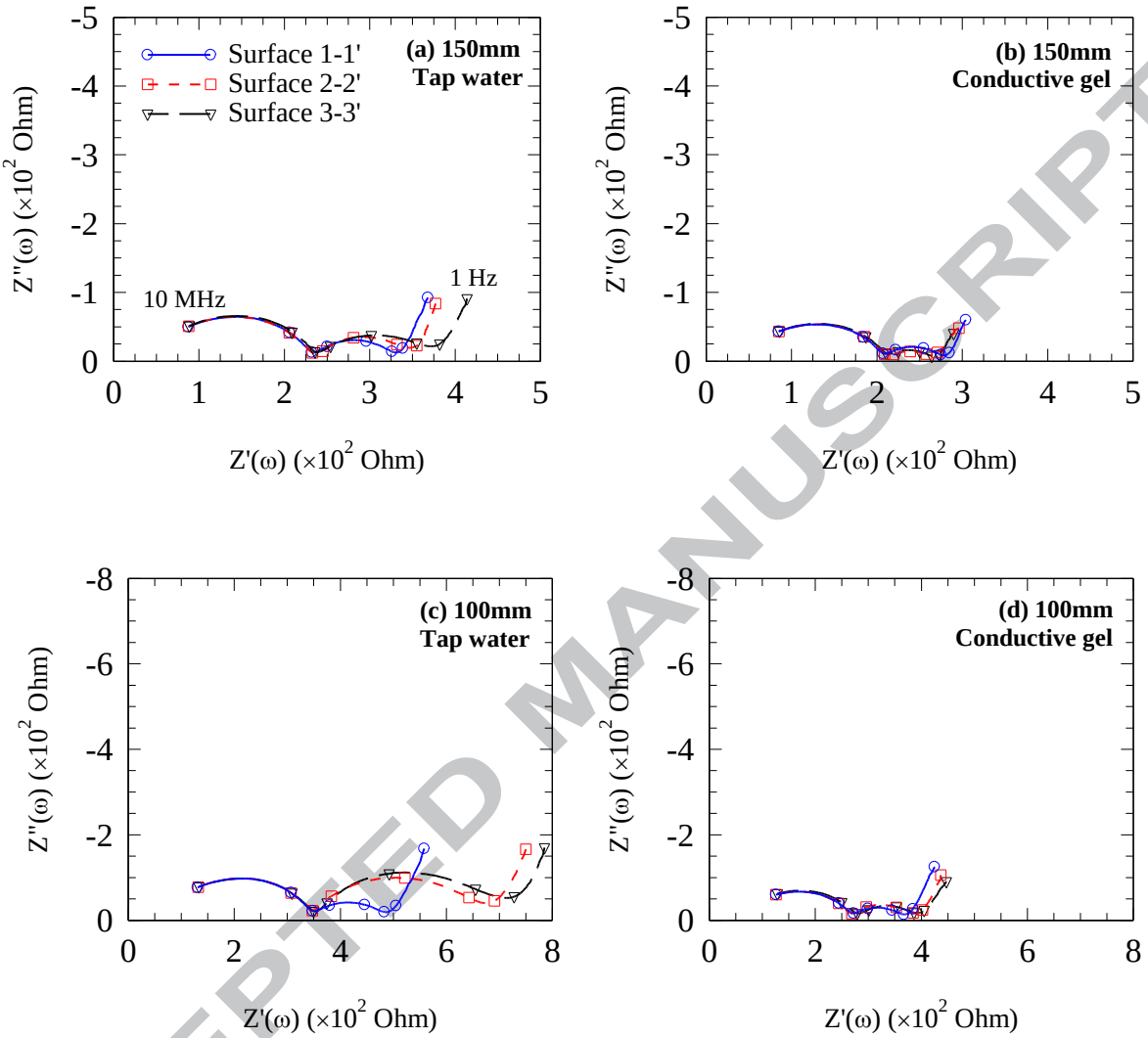

Figure 13. Variations in impedance response for each pair of opposing surfaces for: (a) and (b) 150mm cube; and (c) and (d) 100mm cube.

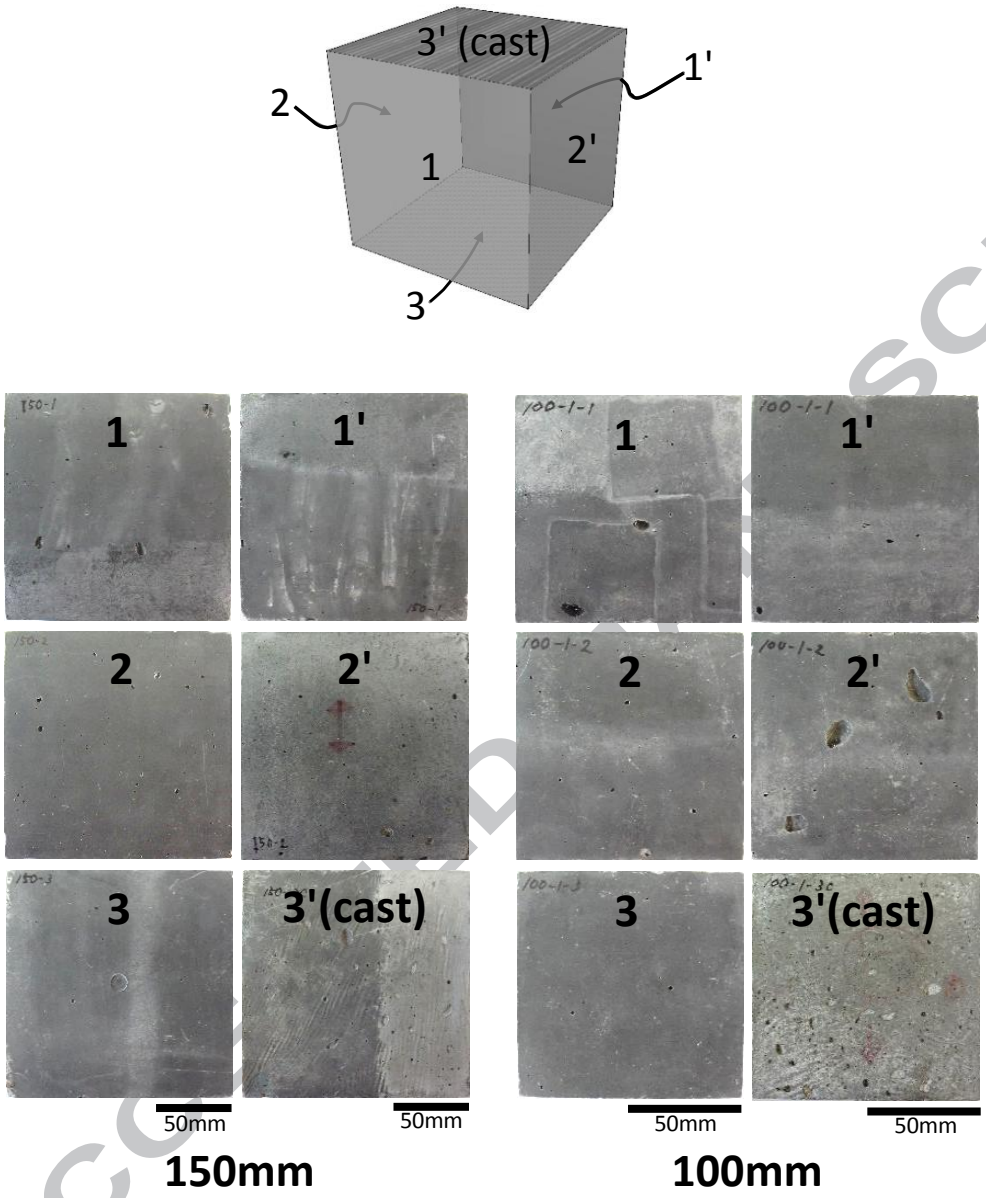

Figure 14. Images of the test surfaces of 150mm and 100mm specimens.

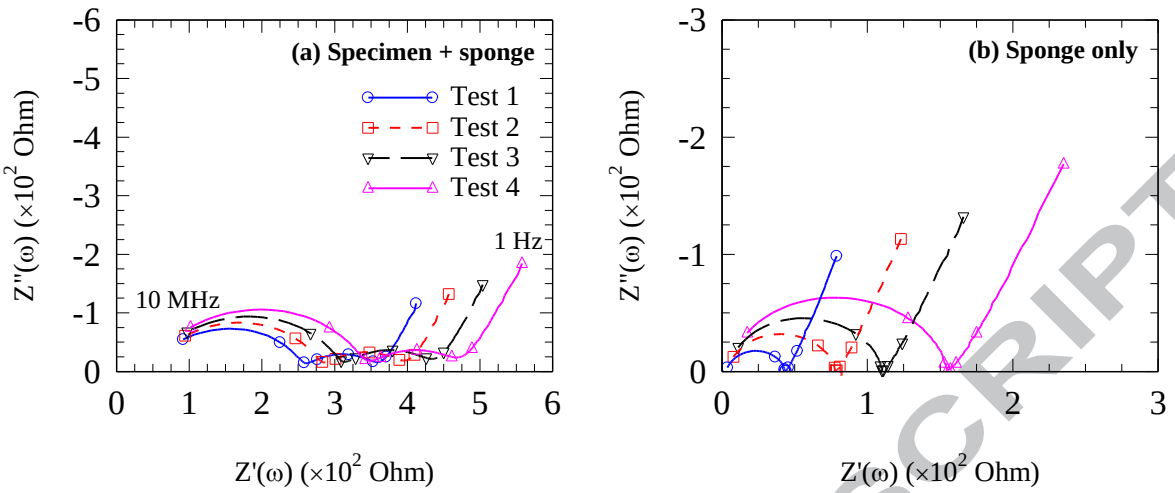

Figure 15. (a) Influence of squeezing on the impedance response of 150mm cube; and (b) the corresponding impedance response of the sponges.

Table captions

Table 1. Empirical concrete resistivity thresholds for protection of embedded steel reinforcement (adapted from [36, 37]).

Table 2. ECC mix used in the experimental programme.

Table 3. Oxide analysis and physical properties of cement, fly-ash and silica sand (wt%).

Table 4. Summary of bulk density and compressive strength. Values in brackets are coefficients of variation (in %).

Table 5. Summary of specimens used in the experimental programme.

Table 6. Summary of salient frequencies on the Nyquist plots presented in Figures 4(a)–(c).

Table 7. Summary of bulk resistivity calculations at 35 days of curing.

Table 8. Summary of bulk resistivity of 150mm specimen taken with sponges of varying degrees of saturation.

Table 1. Empirical concrete resistivity thresholds for protection of embedded steel reinforcement (adapted from [36, 37]).

Resistance to corrosion	**Bulk Resistivity (Ω-m)**
Low	< 50
Moderate / Low	50 - 100
High	100 - 200
Very High	> 200

Table 2. ECC mix used in the experimental programme.

w/b	**CEM I kg/m^3**	**FA kg/m^3**	**Silica kg/m^3**	**HRWR kg/m^3**	**PVA kg/m^3**
0.28	432	777	389	4.3	26

Notes: w/b: water-binder ratio, binder includes cement and fly-ash, HRWR: high range water reducer (BASF MasterGlenium ACE499).

Table 3. Oxide analysis and physical properties of cement, fly-ash and silica sand (wt%).

	Cement	Fly-ash	Silica sand
Chemical analysis			
SiO_2	19.67	52.7	98.8
Al_2O_3	4.84	26.6	0.21
Fe_2O_3	3.17	5.6	0.09
K_2O	0.55	–	0.03
CaO	62.58	2.4	–
MgO	2.22	1.2	–
Na_2O	0.17	1.7	–
SO_4	–	0.3	–
Free CaO	–	0.03	–
Total phosphate	–	0.5	–
Loss on Ignition (LOI)	–	<2.0	0.14
Physical properties			
Specific gravity	3.15	2.20	2.65
Surface area (m^2/kg)	–	1300	–
Fineness (% retained on 25 μm)	–	<25	–
Size distribution (μm) and cumulative retained (%)			
500	–	–	0.1
355	–	–	0.5
250	–	–	1.5
180	–	–	6.0
125	–	–	46.0
90	–	–	83.0
63	–	–	96.5

Table 4. Summary of specimens used in the experimental programme.

Batch	Prism	Cube				Purpose
	40×40×160mm^3	50mm	70mm	100mm	150mm	
1	–	3	3	3	–	Compression tests
2	–	3	3	3	–	Electrical measurements
3	3	3[#]	–	–	1	Electrical measurements Compression tests[#]

Table 5. Summary of bulk density and compressive strength. Values in brackets are coefficients of variation (in %).

Dimension mm	Density kg/m^3	Compressive strength MPa
50	1915 (0.5)	45.1 (1.7)
70	1890 (0.8)	41.1 (3.6)
100	1929 (0.9)	44.4 (2.7)

Table 6. Summary of salient frequencies on the Nyquist plots presented in Figures 4(a)–(c).

Dimension (mm)	Contacting Medium	$f_{c,l}$ $\times 10^2$ (Hz)	$f_{p,m}$ $\times 10^3$ (Hz)	$f_{c,h}$ $\times 10^4$ (Hz)	$f_{p,h}$ $\times 10^6$ (Hz)
50×50×50	Tap water	3.16	7.08	11.2	3.98
	$Ca(OH)_2$	2.51	7.94	14.1	5.62
	Cond. gel	1.26	7.08	12.6	5.62
	CoV (%)	41.9	6.8	11.5	18.7
70×70×70	Tap water	1.26	3.98	7.94	4.47
	$Ca(OH)_2$	1.00	4.47	7.94	5.01
	Cond. gel	0.56	6.31	7.08	5.01
	CoV (%)	37.4	25.0	6.5	6.5
100×100×100	Tap water	0.56	2.24	7.08	3.98
	$Ca(OH)_2$	0.56	2.82	7.08	5.01
	Cond. gel	0.56	3.98	7.08	5.01
	CoV (%)	–	29.5	–	12.7
150×150×150	Tap water	0.45	1.00	5.01	3.98
	$Ca(OH)_2$	0.45	1.58	5.01	3.98
	Cond. gel	0.56	2.82	3.55	3.98
	CoV (%)	13.8	51.5	18.7	–

Table 7. Summary of bulk resistivity calculations at 35 days of curing.

Dimension (mm)	Contacting Medium	Test specimen $Z'(\omega)$ (Ω)	Test specimen $Z''(\omega)$ (Ω)	Test specimen $R_{ECC+cont}$ Eq.4(Ω)	R_{cont} (Ω)	R_{ECC} *Eq. 3* (Ω)	ρ *Eq. 2* (Ω-m)	$\frac{\rho_{ext}}{\rho_{emb}}$
50×50×50	Tap water	845.0	-83.6	853.3	216.6	636.7	31.8	0.99
	$Ca(OH)_2$	700.2	-71.5	707.5	29.7	677.8	33.9	1.06
	Cond. gel	659.8	-62.4	665.7	1.2	664.5	33.2	1.04
70×70×70	Tap water	556.8	-39.9	559.7	106.1	453.5	31.7	0.99
	$Ca(OH)_2$	493.7	-36.5	496.4	15.2	481.2	33.7	1.05
	Cond. gel	490.5	-33.8	492.8	1.5	491.3	34.4	1.07
100×100×100	Tap water	387.0	-23.4	388.4	60.9	327.5	32.7	1.02
	$Ca(OH)_2$	346.0	-21.4	347.3	8.1	339.2	33.9	1.06
	Cond. gel	340.0	-20.5	341.2	1.4	339.8	34.0	1.06
150×150×150	Tap water	280.4	-15.4	281.3	31.7	249.5	37.4	1.17
	$Ca(OH)_2$	259.4	-14.3	260.2	4.6	255.6	38.3	1.20
	Cond. gel	260.7	-12.8	261.3	1.5	259.8	39.0	1.22
40×40×160	Embedded	2796.7	-28.6	–	–	2797	32.0	–
	Embedded	2802.7	-28.5	–	–	2803	32.0	–

Table 8. Summary of bulk resistivity of 150mm specimen taken with sponges of varying degrees of saturation.

Dimension (mm)	Contacting Medium	Test specimen $Z'(\omega)$ (Ω)	Test specimen $Z''(\omega)$ (Ω)	Test specimen $R_{ECC+cont}$ Eq.4(Ω)	R_{cont} (Ω)	R_{ECC} *Eq. 3* (Ω)	ρ *Eq. 2* (Ωm)	$\frac{\rho_{ext}}{\rho_{emb}}$
150×150×150	Tap water	261.8	-14.3	262.6	43.3	219.3	32.9	1.13
	Tap water	287.1	-15.3	287.9	77.8	210.1	31.5	1.08
	Tap water	314.7	-16.5	315.6	109.8	205.8	30.9	1.06
	Tap water	348.6	-18.1	349.5	154.5	195.1	29.3	1.00
40×40×160	Embedded	2551.5	-26.1	–	–	2551.8	29.2	–

Highlights

- A critical evaluation of electrical property measurements on cementitious materials
- Identification of key factors which influence testing procedures/protocols
- A dual bulk-arc response observed in the Nyquist format
- Influence of contacting medium detectable across the entire frequency range
- Interfacial phenomena at the electrode/specimen contact region highlighted